Effect of Catalyst Shape and Etchant Composition on Etching Direction in Metal-Assisted Chemical Etching of Silicon to Fabricate 3D Nanostructures

Owen James Hildreth, Wei Lin, and Ching Ping Wong*

School of Materials Science and Engineering, Georgia Institute of Technology, 771 Ferst Drive, Love Building, Room 288, Atlanta, Georgia 30332

ABSTRACT Metal-assisted chemical etching (MaCE) of silicon in conjunction with shaped catalysts was used to fabricate 3D nanostructures such as sloping channels, cycloids, and spirals along with traditional vertical channels. The investigation used silver nanorods, nanodonuts along with electron beam lithography (EBL)-patterned gold nanodiscs, nanolines, squares, grids, and star-shaped catalysts to show how catalyst shape and line width directly influence etching direction. Feature sizes ranging from micrometers down to 25 nm were achieved with aspect ratios of at least 10:1 and wall roughness of 10 nm or less. This research demonstrates the potential of MaCE as a new, maskless nanofabrication technology.

KEYWORDS: nanofabrication · metal-assisted chemical etching · silicon · etching · 3D nanostructures

There are a number of different techniques to etch nanostructures in silicon for applications in electronic devices,[1] photovoltaic cells,[2] optoelectronics,[3] microelectromechanical (MEM) devices,[4] and more. Wet chemical methods utilizing both acids and bases are widely used to fabricate pyramids, channels, undercuts, and a variety of simple 2D shapes by exploiting the anisotropic etching rates of crystalline silicon. Dry chemical methods such as plasma etching, ion etching, focused ion beam (FIB) milling/deposition, and deep reactive ion etching (DRIE) are used to fabricate micrometer, submicrometer, and nanosized channels and wires into silicon for use in photonic waveguides,[5] metamaterials,[6,7] nanofluidics,[8] and more. While these technologies have successfully been used to fabricate nanostructures of varying degrees of complexity, two fundamental trade offs exist for all current nanofabrication techniques that limit the type of structures that can be fabricated. The first and most inhibiting limitation is that complex 3D shapes are difficult, if not impossible, to make. Wet chemical and dry etching techniques are widely used to form cantilevers and MEMs devices; however, these shapes are generally limited to simple undercuts of 2D patterns and require multiple, iterative lithography, etching, and deposition steps.[9,10] The second limitation is that, as feature sizes shrink into the nanosize domain, it becomes increasingly difficult to accurately maintain those features over large depths and heights; features can be created with either high complexity but low aspect ratios on the order of 7:1[6,11] or with low complexity and high aspect ratios.[12] DRIE is generally used to create structures with aspect ratios of around 10:1 under general conditions, although it has been used to create high aspect ratio silicon nanowires with aspect ratios of 50:1;[12] however, the process leaves rough, scalloped side walls and requires specialized equipment. Which can limit both device efficiency and widespread adaption by industry.

To overcome the limitations of current nanofabrication technologies, the authors have started to develop a new nanofabrication technique using metal-assisted chemical etching (MaCE) in conjunction with controlled catalyst shapes to etch 2D and 3D patterns into silicon. In this study, we examine the influence of catalyst shape and etchant composition on etching direction to fabricate 3D cycloids, spirals along with slanted and vertical nanochannels with aspect ratios of at least 10:1 using MaCE.

MaCE is an electroless chemical etching technique that can etch micrometer, submicrometer, and nanosized features in silicon with high aspect ratios and has been widely used to fabricate photoluminescent silicon,[13,14] Si nanowires,[15] and super hydrophobic structures.[16,17] MaCE traditionally

*Address correspondence to cp.wong@mse.gatech.edu.

Received for review September 7, 2009 and accepted November 19, 2009.

Published online December 2, 2009.
10.1021/nn901174e

© 2009 American Chemical Society

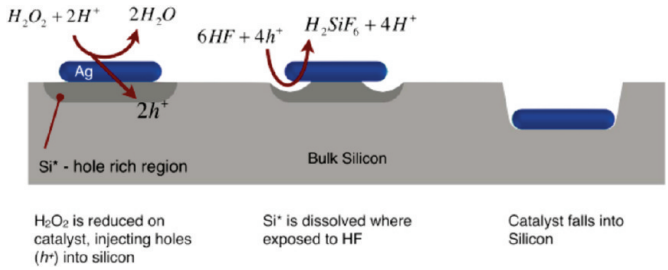

Scheme 1. Schematic of the etching process. H_2O_2 is reduced at Ag nanorod injecting holes (h^+) into the silicon valence band, creating a hole (h^+)-rich region around the catalyst particle. The holes (h^+) are consumed by the oxidation of Si^0 to Si^{4+} at the HF interface to form soluble SiF_4^{2-}. The Ag nanorod travels into the silicon wafer as silicon around and beneath the nanorod is dissolved.

uses nanoparticles or discontinuous thin films of Ag, Au, or Pt to locally increase the silicon dissolution rate in a solution of hydrofluoric acid (HF) and hydrogen peroxide (H_2O_2) or other oxidizing agent. The proposed mechanism involves a local coupling of redox reactions[14] and is schematically illustrated in Scheme 1 with Ag nanorods as the catalyst. The etching process begins as H_2O_2 is catalytically reduced at the Ag nanorod, creating a local cathode on the etchant side of the Ag nanorod that injects holes (h^+) into the valence band of the Si, leading to a hole (h^+)-rich region of silicon (Si*) surrounding the Ag nanorod catalyst. Holes (h^+) are consumed at the HF/Si* interface in the oxidation of Si^0 to Si^{4+} to produce soluble SiF_6^{2-} and H_2SiF_6. The etching process continues as the Ag nanorod travels into the regions where the silicon around and beneath the Ag nanorod is dissolved. Depending primarily on etchant composition, the silicon dissolution will either be limited to regions within a few nanometers or less of the catalyst particle, creating very narrow holes, or silicon dissolution can take place tens to hundreds of nanometers or more away from the catalyst particle, creating conical holes.[18]

Unlike other etching techniques, where a pattern of material remains on the top surface acting as a mask, in MaCE, the metal catalyst moves into the substrate as the silicon around and beneath the catalyst dissolves. Because the catalyst can travel in three dimensions while continuing to etch, it is possible to create 3D patterns in the silicon with straight,[19] curved,[20] helical,[21] and random[20] etching paths reported for Pt, Au, and Ag nanoparticles and colloids. MaCE has widely been used to create high aspect ratio holes in silicon on the order of 10:1[19−21] to greater than 40:1.[22] While the influence of etchant composition on hole morphology and shape has been widely studied for nanoparticles and noncontinuous thin films, there has been no research on the effect and importance of catalyst shape on etching direction and, except for a brief study by Li *et al.*,[23] no effort has been made to use MaCE as a method to fabricate complex 2D and 3D structures with high feature resolution. In this study, we show that catalyst shape, catalyst fabrication method, and etchant composition significantly influence etching direction. We also demonstrate that MaCE can be used to etch nanostructures not only perpendicular to the substrate surface but also 3D spirals, twists, cycloids, slanted channels, and "S-shaped" undercuts with feature sizes ranging from hundreds of nanometers down to tens of nanometers. The side walls are shown to be smooth with an estimated ~5−10 nm of roughness based upon SEM image.

TABLE 1. Etchant Compositions Used[a]

	volume (mL)			molarity (M)		
ρ	HF (49%)	H_2O_2 (30%)	H_2O	HF	H_2O_2	H_2O
90	4.0	1.2	1.7	16.7	1.8	36.6
60[b]	4.0	7.2	1.1	9.4	6.2	36.8
40	4.0	15.6	0.0	5.9	8.4	36.6

[a]Where ρ = [HF]/([HF] + [H_2O_2]) with volumes used and molarities of HF (Aldrich, 49%), H_2O_2 (Aldrich, 30%), and H_2O (distilled). [b]Where ρ = 60 was only used for Au grid catalysts.

RESULTS AND DISCUSSION

Two different catalyst fabrication methods were used: wet chemical synthesis of Ag nanorods and Ag nanodonuts along with electron beam lithography (EBL)-patterned Au nanostructures. Using different fabrication methods allowed us to not only create a variety of complex shapes but also examine the influence of side wall shape with round Ag nanorods etching both cycloids and straight paths while EBL-patterned nanolines etched more erratic etching paths. Results with the EBL-patterned catalyst also show how both the shape of the catalyst and the ratio of catalyst line width *versus* thickness directly influence etching direction. All samples were prepared on a 100 mm, single side polished, p-type (1−100 Ω) single-crystal (100) silicon wafer, which was imaged perpendicular to the silicon surface before or after etching using a thermally assisted field emission scanning electron microscope (SEM) at 10 kV, which provides a subsurface image contrast for Ag and Au of an estimated 300 nm.[24]

We have adopted the etchant composition notation used by Lévy-Clément *et al.*,[18] where ρ = [HF]/([HF] + [H_2O_2]) with [H_2O] kept constant. The volumes and molarity of HF, H_2O_2, and H_2O corresponding to each etchant composition are shown in Table 1. Care was taken to ensure that the etchant solution flowed slowly over the silicon wafer; otherwise, the solution can move the catalyst during the etching process. The etchant solution was kept stagnant during etching, and the only opportunities for external excitation were when the etchant was applied and removed from the sample.

Etching Path of Ag Nanorods and Nanodonuts. Ag nanorods were fabricated be reducing $AgNO_3$ in a solution of ethylene glycol using poly(vinyl pyrrolidone) (PVP) as the capping agent[25] and then centrifuged 6−10 times

in ethanol to remove excess PVP and ethylene glycol. The Ag nanorods were then diluted with ethanol to form a lightly colored solution and placed onto the silicon wafer to form a thin film that did not break apart during drying. Once dry, the samples were placed into a UV−ozone stripper to remove the PVP capping agent prior to etching. Ag nanodonuts were fabricated using the same chemical methods as the Ag nanorods but at higher temperature to form submicrometer particles that were then aged for 1 month before being deposited onto the silicon wafer and distorted into a donut shape using UV−ozone. All Ag nanorod samples were etched for 10 min with $\rho = 90$ etchant.

Ag nanorod catalysts produce straight and cycloid channels with widths and lengths that fall within the diameter and length distributions for the post-UV−ozone-treated Ag nanorods. For this paper, the term "cycloid" is used loosely to indicate that the Ag nanorod etched below the silicon surface and then changed direction to etch through to the top surface, reemerging some distance away as shown in Figure 1a. The SEM image shows a top-down view of a ~70 nm wide, 1.4 μm long cycloid with a 380 nm pitch. The etching path is schematically illustrated in 3D and 2D in Figure 1b,c; white, dashed circles were added to each image to show the subsurface "/\" wedge shape created as the Ag nanorod etched upward, through the surface and then back down again; the Ag nanorod can be seen just below the Au-coated silicon surface on the right of Figure 1a. The SEM images in Figure 1 are typical of UV−ozone-treated Ag nanorod catalysts in a $\rho = 90$ etchant and show both cycloid and straight channels. The width of the etched channels ranges from ~60 to 100 nm, and they are between 500 nm and 1.5 μm long. Figure 1d shows a region with predominately cycloid etching, while Figure 1e,f shows straight channels around 30−40 nm wide. For most Ag nanorod cycloids, etching was confined to a plane perpendicular to the longitudinal axis.

Ag nanodonuts were synthesized using the same solution-based method as Ag nanorods with some modifications. The reaction was conducted at 170 °C instead of 160 °C, then the solution was separated and cleaned *via* centrifugation using the same conditions before being stored in ethanol for 1 month in the dark before UV−ozone cleaning. Depending on position in the UV−ozone stripper, time, and particle size, a portion of the submicrometer Ag particles distorted to form Ag nanodonuts. This process also removes any PVP capping agent and cleans the catalyst for MaCE. The nanodonuts were etched at $\rho = 90$ for 30 s and 10 min. Figure 1g−i shows the submicrometer Ag particles before UV−ozone and then as nanodonuts after 30 s and 10 min of etching. The etched profile conforms to within the SEM resolution limit of 10 nm. Notice that the etching path is almost perpendicular to the surface with some slight rotation about the *Z* axis.

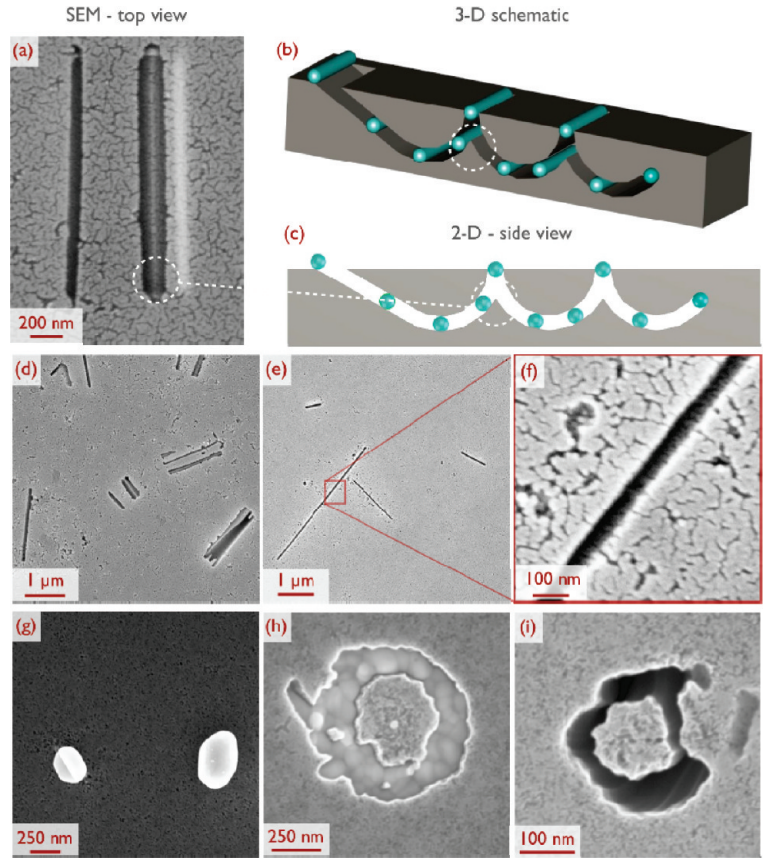

Figure 1. Etching with Ag nanorods and nanodonuts after UV−ozone PVP removal using $\rho = 90$ etchant for 10 min. (a) Top view SEM image. Ag nanorod started at left-hand hole, etching into silicon and re-immerged 300 nm and then etched back into silicon. Ag nanorod can be seen just below the Si surface on far right. (b) Three-dimensional schematic of etching path. (c) Two-dimensional side view schematic of etching path. The white dashed circles on the images highlight the silicon wedge remnant just below the top surface on all three images. (d) Cycloid-like and straight paths; width of nanorod channels range from ~60 to ~80 and 500 nm to 1.5 μm long. (e) Straight channels between 30 and 60 nm wide and 430 nm and 3.4 μm long. (f) Higher magnification of image (e) showing ~30 nm wide channel. Samples were coated with ~5 nm of Au after etching for enhanced (g) submicrometer Ag particles before UV−ozone treatment; (h) Ag nanodonut just below the Si surface. Notice that the etched hole matches that of the catalyst particle; (i) etching path of Ag nanodonut after 10 min of etching. Notice that the etching path is predominately perpendicular to the surface with some slight twisting.

The cycloid-like etching shown in Figure 1 demonstrates that gravity is not the only force acting on the Ag nanorods during etching. In Peng *et al.*'s examination of the motility of Ag nanoparticles during MaCE, they proposed that the coupled anodic and cathodic reactions generate an electric field across the metal nanoparticle, which results in self-induced electrophoretic motion toward the silicon anode with the Ag particle slip velocity given by the Hünkel equation below.[26]

$$v_{ep} = \frac{2\varepsilon\zeta E_{||}}{3\eta} \quad (1)$$

where υ_{ep}, ε, ζ, η, and $E_{\parallel}$ are the slip velocity of the particle, the permittivity of the solution, the zeta potential of the Ag nanoparticle, the viscosity of the solution, and the electric field parallel to the particle surface, respectively. While the electrophoretic mechanism was not rigorously proven, the cycloid-like etchings shown in Figure 1 do support their hypothesis. It is clear from Figure 1h that, under $\rho = 90$ etchant, the shape of the etched channel tightly conforms to the shape of the catalyst, and the distance between the sides of the catalyst and the walls is on the order of 10 nm or less; thus, it is reasonable to assume that the top half of the catalyst particle acts as an anode, while the bottom half of the particle acts as the cathode and that the net $E_{\parallel}$ and υ_{ep} of a Ag nanoparticle differ from those of a nanorod with the $E_{\parallel}$ of a nanorod primarily directed perpendicular to the longitudinal axis. The origin of the cycloid-like motion can be explained by the inclusion of local perturbations such as non-uniform instantaneous reduction and oxidation rates or accelerations due to Brownian motion. These perturbations may instantaneously change the etching direction or the net electric field, causing the catalyst to change direction, which also changes the sections of the catalyst exposed to the etchant solution and silicon. Once new anode and cathode regions have been established, the new $E_{\parallel}$ and υ_{ep} will propel the catalyst in a different direction. Thus, small perturbations can cause a change in direction with electrophoresis providing the forces necessary to overcome gravity and Brownian motion. To better explain this phenomenon, more complicated and exact theory is needed that takes into account factors such as etchant composition, reactant and product diffusion, hydronium ion migration, Brownian motion, hole (h^+) diffusion in silicon, and more.[27] For this moment, the authors cannot provide detailed proof of the above hypothesis; however, upon the basis of the available data, electrophoresis does appear to be a likely candidate for catalyst motion, and a more fundamental study of catalyst motion in MaCE is currently underway.

Our results show that trends exist between catalyst particle shape and etching path with certain shapes showing a reduction in translational and rotational freedom even though there are no physical constraints within the silicon. As shown in Figure 1 and SI-Figure 10 (Supporting Information), both Ag nanorods and nanodonuts show very different etching paths under these etching conditions, especially when compared to the etching paths of nanoparticles reported by others.[15,19] As mentioned previously, changes in catalyst shape effect the shape and direction of the electric field responsible for electrophoretic motion. For certain shapes, such as Ag nanorods, the electrophoretic forces loosely confine the catalyst particle along certain planes and directions in a manner that is akin to removing degrees of translational and rotational freedom. For example, under $\rho = 90$, nanoparticles will etch random paths through the silicon, capable of moving with a full 6 degrees of freedom (DoF), while Ag nanorods are predominately confined to a plane perpendicular to the longitudinal axis, giving them 3 DoF: two translational, one rotational. Ag nanodonuts exhibit 2 DoF, capable of etching perpendicular to the substrate with some slight rotation about an axis also perpendicular to the substrate. These changes in DoF are most likely due to changes in the electric field and electrophoretic motion caused by the change in catalyst shape; however, other factors such as concentration gradients, Brownian motion, diffusion, and diffusion paths may also play a critical role in determining etching direction.

Etching Path of Au Nanolines and Dog-Bone Shapes. The etched paths made using Ag nanorod and nanodonut catalysts showed that catalyst shape directly influences etching direction. To study more complex shapes, we used EBL to fabricate Ti/Au nanostructures with a 10 nm base adhesion layer of Ti followed by 50 nm of Au catalyst consisting of discs, lines, "dog-bone" shapes, squares, stars, and grids with line widths ranging from 25 to 200 nm and lengths from 200 nm to 5 μm. A schematic illustrating the EBL patterning and etching process along with an SEM image of the patterns prior to etching can be found in the Supporting Information. In our initial tests, we found that the Ti adhesion layer lowered the etching rate and all EBL samples were etched for 40 min in $\rho = 40$ and 90 etchant. For brevity, the only $\rho = 60$ etchant results reported are for the spiral etching seen for filled catalysts (Figure 6b,c) because they clearly demonstrate the 3D etching capabilities of MaCE.

The importance of cross-section shape, profile shape, and line width to thickness ratio on etching direction is clearly demonstrated in Figure 2, which shows the etching path of Au nanolines and dog-bone shapes with line widths ranging from 200, 100, 50, and 25 nm in $\rho = 40$ and 90 etchants. The change from the circular cross section of Ag nanorods to the rectangular cross section of Au nanolines (Figure 2c,e) dramatically changed the etching path, and clean cycloid-like paths were rarely seen. Instead, the Au nanolines appear to remain closer to the surface with 200 and 100 nm line widths slicing just below the surface, while 50 and 25 nm line widths appear to penetrate farther into the silicon and resurface less frequently. Etchant composition also changes the etching path of the nanolines, and the $\rho = 40$ etchant created less erratic etchings with 200 nm line widths sliding along the silicon surface, 100 nm line widths sliding just below the surface with some bending, while the 50 and 25 nm line widths appear to cycle near the surface a couple of times before etching deep into the silicon. In contrast, the $\rho = 90$ etchant showed very erratic etching along with considerable catalyst distortion, bending, and even tumbling. One possible explanation for this more erratic etching is that the difference in etchant composition changes both

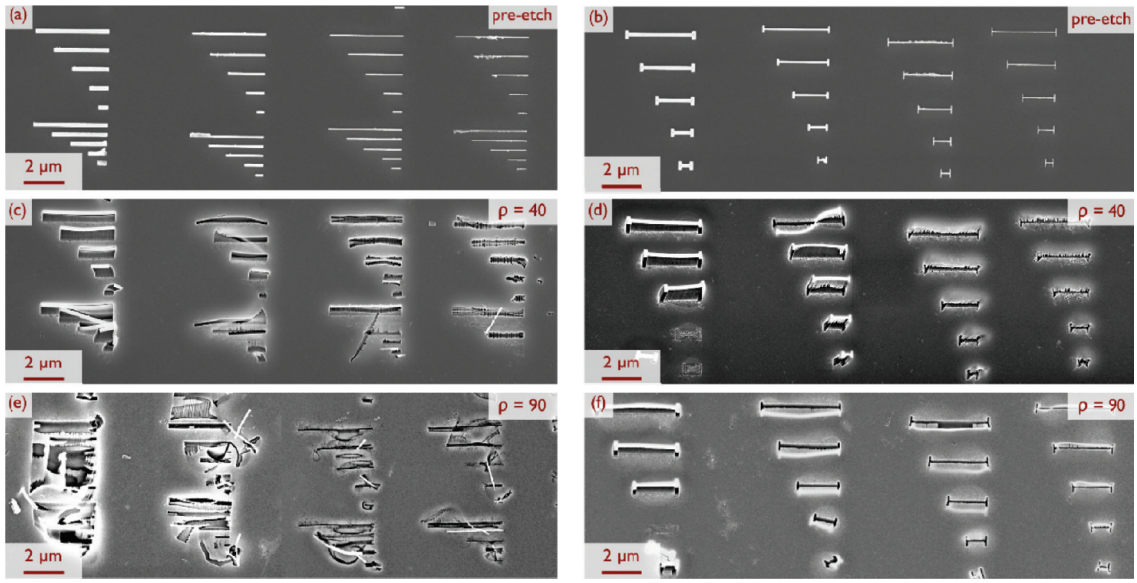

Figure 2. SEM images of silicon etched with EBL-patterned Au catalysts for 40 min. Left column is Au nanolines. Right column is Au dog-bone shapes. Line widths are 200, 100, 50, and 25 nm from left to right.

the etching rate of the silicon and the electric field strength across the catalyst particle, which, as proposed by Peng *et al.*, is responsible for the self-electrophoresis movement seen by metal nanoparticles in MaCE of silicon.[26] Although it is clear that etchant composition affects etching path, exactly how this occurs and whether or not other factors exist beyond the electric field and the resulting migration velocity still needs to be determined. The bending and tumbling paths were rarely seen with Ag nanorods, and the changes in catalyst composition and the area moment of inertia may also play a role in determining etching direction.

The small addition of 400 nm long end caps to the Au nanolines to create Au dog-bone catalyst completely eliminated the cycloid-like etching seen with Ag nanorods and Au nanolines. The effect of line width on etching direction is clearly seen in Figure 2e,f, with 200 nm wide catalysts etching shallow, sliding paths, 100 nm wide catalyst etching at a larger sliding angle with the catalyst completely below the silicon surface, the 50 nm wide catalyst etch at an even steeper angle, and lastly, the 25 nm wide catalysts were bent in the $\rho = 90$ etchant while straight, vertical paths were observed for $\rho = 40$. Unlike Au nanodiscs and nanolines, the dog-bone shapes do not change etching direction, even if the catalyst is bent, as such they have 2 translational DoF before etching starts confined to the *Y* and *Z* planes perpendicular to the long axis; however, because the dog-bones do not change direction once etching starts, the catalyst is confined to a 1/2 DoF along the initial direction of motion directed into the bulk silicon.

Etching Path of Au Squares and Grids. Square catalyst continued the etching trend of Au dog-bones with more complex shapes creating additional boundary conditions that restrict catalyst motion to some degree. From top to bottom, each row of Figure 3 shows the etching path of ~25, ~50, and ~100 nm line width catalysts while the left and right columns are $\rho = 40$ and 90 etchants, respectively. The insets show the original catalyst before etching. Once again, the ~25 and ~50 nm line width catalysts etched paths either perpendicular

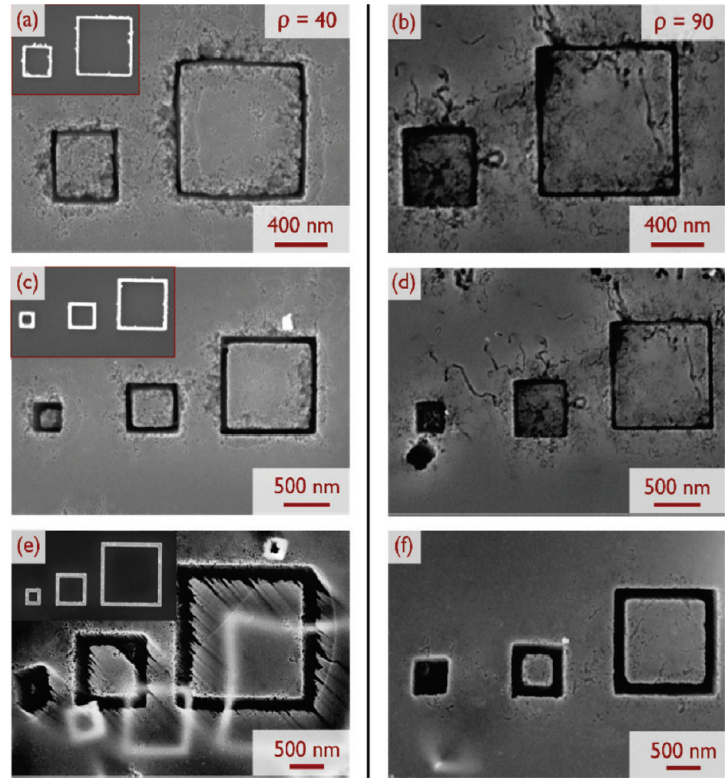

Figure 3. SEM images of Si etched with Au squares for 40 min. Left column is etched with $\rho = 40$ etchant, right column is etched with $\rho = 90$ etchant: (a) 25 nm line width, $\rho = 40$; (b) 25 nm line width, $\rho = 90$; (c) 50 nm line width, $\rho = 40$; (d) 50 nm line width, $\rho = 90$; (e) 100 nm line width, $\rho = 40$; (f) 100 nm line width, $\rho = 90$.

or nearly perpendicular to the surface, while the 100 nm line width catalyst etches at an angle, creating sloping channels and reinforcing the idea that line width plays an important role in determining catalyst direction. All of the 25 and 50 nm wide catalysts etched beyond the secondary electron escape depth of ~300 nm for silicon (estimated),[24] providing an aspect ratio of ~6:1 or greater for the 25 nm wide catalysts. The square catalysts with 100 nm line widths can be seen beneath the silicon surface for the $\rho = 40$ etchant (Figure 3e); the smaller, 350 nm and 1 μm long squares are not deformed, while the longer 2 μm square is; this indicates that, as expected, the long, narrow structures are more prone to distortion during the etching process. In order to fabricate long, narrow nanostructures, it will be necessary to further study and understand the forces involved in MaCE. How are they created and what etchant conditions provide an optimum balance between electrophoretic slip velocity and catalyst distortion?

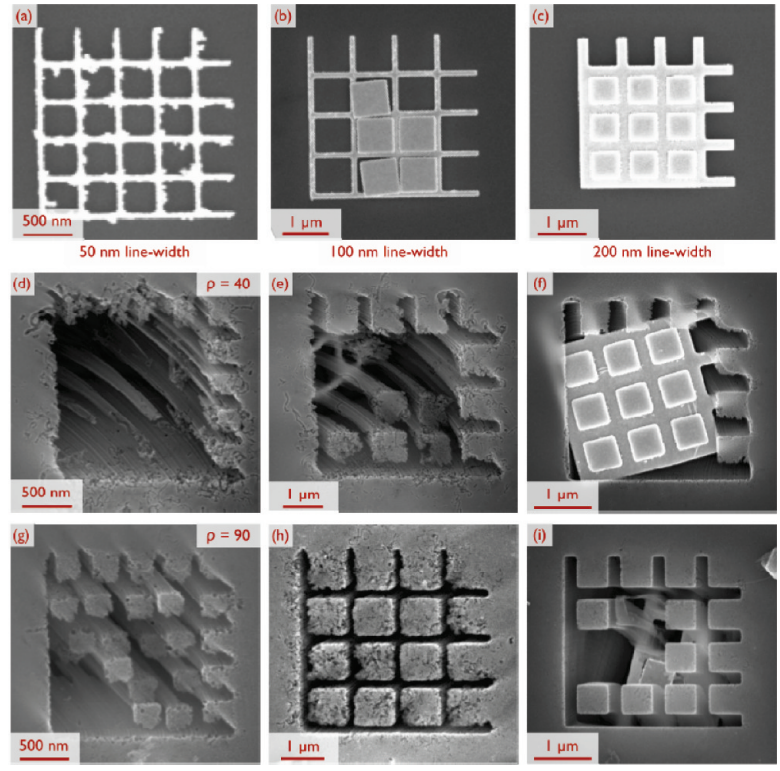

Figure 4. SEM image of silicon etched with Au nanogrids for 40 min. The rows from top to bottom correspond to pre-etch catalyst, ρ = 40 etchant or ρ = 90 etchant. The columns from left to right correspond to 50, 100, and 200 nm line widths. Better feature resolution of the standing silicon pillars is seen for the 90 etchant.

A close inspection of internal shadows in the channels of Figure 3f shows that each nanosquare catalyst etches in a different direction and angle; the 350 nm long catalyst etched toward the bottom right ($+X$, $-Y$, $-Z$), the 500 nm long catalyst toward the bottom left ($-X$, $-Y$, $-Z$), and the 1 μm long catalyst toward the upper left ($-X$, $+Y$, $-Z$). These results show that MaCE is a dynamic process that depends not only on catalyst shape, etchant composition, temperature, *etc.* but also on local, dynamic changes in etching rates and forces which allow each catalyst particle to etch independently. Looking at the side walls in Figure 3f shows that the walls are very smooth with straight lines just above the SEM resolution limit of a few nanometers etched into the walls.

Grid catalysts with 50, 100, and 200 nm line widths etch straight, sliding, and spiral shapes that depend primarily on the line width of the catalyst and if the lift-off process left the center squares filled with gold or not. The Au grid patterns are shown in Figure 4a−c. For the grid catalysts, the etching direction does not appear to depend as much on line width as the Au nanolines and dog-bone shapes; instead, all catalysts appear to etch at an angle while some catalysts rotate about the Z axis also. Both of the 50 nm line width catalysts show relatively smooth walls; however, it is clear from Figure 4a that the 50 nm line width catalyst had very rough edges as compared to the 100 and 200 nm line width catalysts. The catalysts for the 100 nm line width, $\rho = 40$ etchant (Figure 4e), and the 200 nm line width, $\rho = 90$ etchant (Figure 4i), are still visible in the SEM image, and the curved path that the catalysts took can be seen by the curvature of the silicon pillars. While we did not intend to fabricate curved structures, these results clearly show that simple 3D structures can be fabricated using MaCE, and once the factors that influence etching direction have been studied, there is the possibility that evermore complex 3D geometry may be possible by controlling etching parameters such as catalyst shape, composition, multiple layer catalysts, etchant composition, temperature, and more. Extremely smooth walls are clearly shown in all SEM images, with Figure 4f,i being the smoothest.

A study by Lévy-Clément *et al.*[18] on the effect of etchant composition on etching morphology suggests that increasing the $[H_2O_2]$ increases the hole (h^+) injection current and increases the distance holes (h^+) can travel within the silicon before being consumed at the Si*/HF interface, leading to straight, tight holes, to conical holes, craters, and finally polishing regimes for very high H_2O_2 concentrations. Comparing the shape of the silicon pillars left behind on 50 and 100 nm line width catalysts under the $\rho = 40$ and 90 etchants (Figure 4e and Figure 4h,i, respectively) agrees with Lévy-Clément's analysis. The silicon pillars formed in the low

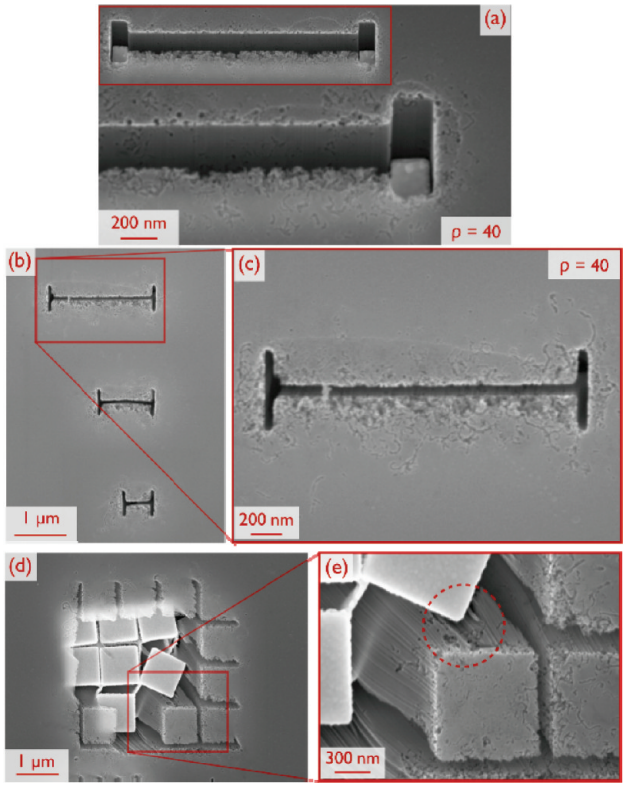

Figure 5. SEM images showing smooth walls and high feature fidelity created using MaCE with ρ = 40 etchant: (a) 200 nm wide Au dog-bone etching at slight angle perpendicular to the surface. Notice the sharp angles and straight side walls. Inset shows the entire 1.5 μm long, 200 nm wide Au dog-bone. (b) Three 50 nm wide Au dog-bones etched almost perpendicular to silicon surface. (c) High magnification image of 50 nm wide, 1.5 μm long channel etched with Au dog-bone etched almost perpendicular to the surface. Slight angle can be seen in the shadow on right and left ends of the channel. (d) Grid pattern with 50 nm line width with sections of fill-in squares. (e) Higher magnification with an estimated roughness of ~10 nm or less. Notice the high feature resolution of MaCE with the etched channel matching the shape of the catalyst within the 10 nm resolution of the SEM.

$[H_2O_2]$ (ρ = 90) etchant maintain their width over the entire length, while the pillars formed in the high $[H_2O_2]$ (ρ = 40) etchant appear to narrow toward the base with significantly more top-surface damage on the pillars than in the surrounding bulk silicon. This indicates that not only are more holes (h^+) generated with ρ = 40 etchant but that holes (h^+) generated near the silicon pillars are at least somewhat confined within the pillars, leading to a higher etching rate for the silicon pillars even after the catalyst particle has etched well over 1 μm away. For MaCE to be used as a nanofabrication method, it will be necessary to study the effect of etchant composition on the resulting structure in more detail at an experimental and theoretical level. However, we have found the ρ = 90 etchant to be a good etchant to start with for high feature resolution, although, as we showed for Au nanolines and dog-bones, the forces on the catalyst at ρ = 90 appear to be either stronger or non-uniform, which can increase the amount of catalyst distortion during the etching process. Nanogrids have 3 translational DoF with some rotational freedom about the *Z* axis.

Feature Resolution and Spiral Etching. The smooth walls and high feature resolution capabilities of MaCE are demonstrated in Figure 5, where top-down SEM images of channels etched with Au dog-bone grids with ρ = 40 etchant have feature resolutions on the order of 10 nm or less. The 200 nm wide, 1.5 μm long Au dog-bone catalyst in Figure 5a shows sharp corners and smooth side walls over its entire length with small, ~10−20 nm pits etched into the side walls. The rougher edge, in the −*Y* direction, shows small pores in the silicon indicating increased silicon etching on the leading edge of the catalyst than the tailing end. Because the etching process is regulated by the local availability of holes (h^+), these results suggest that the leading edges either experience a higher hole (h^+) injection current or that, due to the wedge geometry, (h^+) become confined within this narrow region, leading to a porous structure. Clearly more fundamental studies are needed to explain these results. Figure 5b shows three channels 50 nm wide ranging from 500 nm to 1.5 μm long all etched to depths greater than 200 nm based upon secondary electron escape depth at 10 kV given these features' aspect ratios of at least 4:1. The higher magnification in Figure 5c shows 50 nm wide features etched into silicon. Figure 5e shows a higher magnification image of Figure 5d, where a grid catalyst with a 50 nm line width and incomplete lift-off etched into the silicon. The higher magnification image once again shows relatively smooth walls; however, the etched channel caused by the Au remnant square widens toward the base, indicating

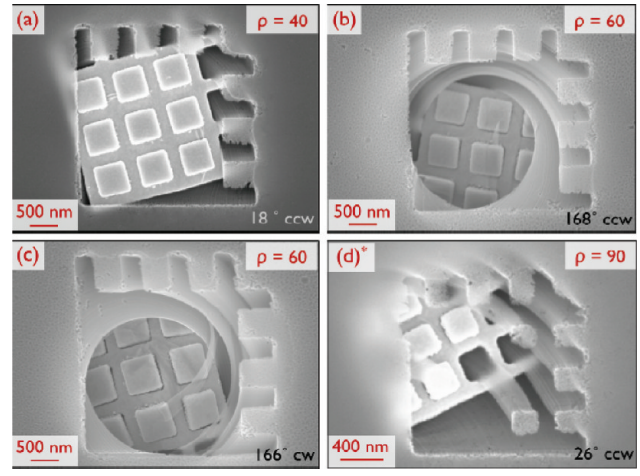

Figure 6. SEM images of spiral etchings paths in silicon etched with Au nanogrids for 20 min under various etchants: (a) ρ = 40 etchant, 18° ccw about centroid axis; (b) ρ = 60 etchant, 162° ccw about centroid axis; (c) ρ = 60 etchant, 168° cw about centroid axis; (d*) ρ = 90 etchant, 26° ccw about noncentroid axis.

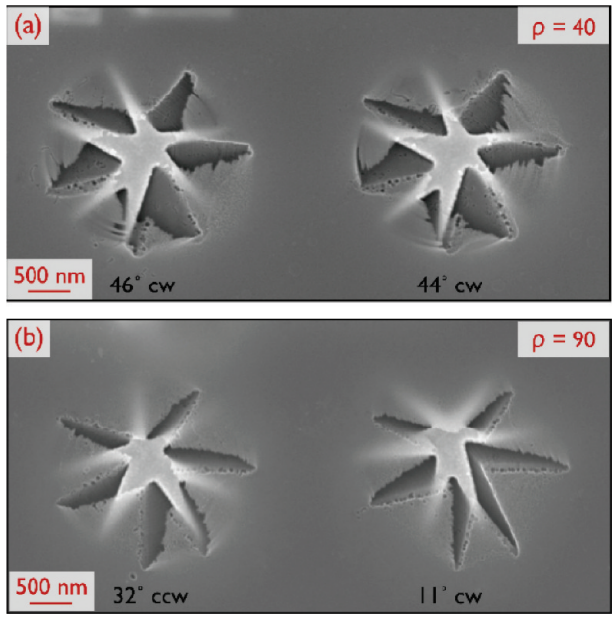

Figure 7. SEM images of spiral etching paths in silicon etched with Au nanostars for 20 min under various etchants. All starts roughly rotate about centroid (a) ρ = 40 etchant, 46° cw and 44° cw, (b) ρ = 90 etchant, 32° ccw and 11° cw rotation with translation in the +*Y* direction.

that the Au square's path differed from that of the Au grid. Although this result was not intended, it does highlight some of the interesting possibilities of MaCE in which the motion of multiple catalysts are coordinated to fabricate increasingly complex structures.

In general, 3D spiral etching was seen for filled-in catalysts with protrusions. Spiral etching of fill-in grid catalysts with 200 nm line widths etched for 20 min in ρ = 40, 60, and 90 etchants is shown in Figure 6. The rotation angles ranged from 18 to 168° in both cw and ccw directions. Most fill-grid catalyst spiraled about an axis near the centroid, although noncentroid rotation was also seen (Figure 6d). AFM measurements of Figure 6b show that the catalyst is 2.1 to 2.5 μm deep (see Supporting Information). The line widths of the spiral arms are 200 nm, providing an aspect ratio of at least 10:1; which is not only comprable to DRIE but MaCE does not leave the rough scalloping seen with DRIE. No conclusions on the effect of etchant composition on spiraling can be made because only few grid patterns remained filled after the lift-off process. Spiraling without translation was only seen for filled or nearly filled catalyst grids; these catalyst structures have no translational DoF and 1 rotational DoF about the *Z* axis. Only one spiral structure was seen for catalysts without protrusions.

Almost all the star-shape catalysts etch spiraling 3D patterns that rotated about the +*Z* or −*Z* axis as they etched into the silicon. As shown in Figure 7, the star shapes in the ρ = 40 etchant rotated 46 and 44° cw about an axis near their centroid with little translation in any direction other than −*Z*. The star-shape catalysts in the ρ = 90 etchant rotated 32° ccw with no translation in *X* or *Y* directions, while the other catalyst rotated 11° cw with 80 nm of translation in −*X* and 220 nm in +*Y*. The ρ = 40 etchant shows lower feature resolution and an increase in nonlocalized etching in the spiraling directions, suggesting that the hole (h^+) density is higher in these areas. Overall, star-shaped catalysts have no translational DoF and 1 rotational DoF about the *Z* axis.

CONCLUSIONS

In this paper, we sought to demonstrate the potential of MaCE as a maskless nanofabrication technology capable of creating high-quality 2D and 3D nanostructures in silicon by examining how catalyst shape directly influences etching direction while etchant composition can influence both feature resolution and, to a lesser degree, etching direction. Starting with Ag nanorods, we showed that both cycloid and straight channels can be fabricated and that Ag nanorods have only 3 DoF as compared to the round particles used in literature, which have a full 6 DoF. Ag nanodonuts were used to show that donut-like structures have only 2 DoF that can rotate as they etch into silicon, leaving behind spiral lines in the shaped template. Au nanolines also had only 2 DoF and showed the effect of side wall shape with straight, sliding, and cycloid-like etching seen. The change from nanolines to more complex shapes such as dog-bones, squares, and grids showed a remarkable change in etching direction and provided insight into the importance of line width on etching direction. First, no cycloid etching was seen for any shapes more complex than a nanoline. Second, the catalysts with 25 and 50 nm line widths, which is less than the 60 nm catalyst thickness, almost always etched vertical or near vertical etching paths, while the thicker 100 and 200 nm line widths etch at large sliding angles. The effect of etchant composition on etching resolution and morphology was best shown using Au nanogrids with the ρ = 40 leading to a larger amount nonlocalized, which provides insight into the location of hole (h^+) rich regions of the silicon. Whether these hole (h^+) rich regions influence etching direction through electrophoretic forces remains unknown. Spiral etching was seen for filled catalysts with protrusions, specifically, the nanogrids with incomplete lift-off and the on-purpose star shapes. These shapes showed that more complex, 3D etching structures can be fabricated and hint at the possibilities that MaCE has for 3D nanofabrication. The ability to etch spirals, cycloids, sliding channels, and other 3D shapes on a nanoscale is unique to MaCE and could be used to fabricate photonic crystals, MEMs devices, and more.

It is clear that etching direction depends on catalyst shape; however, a full understanding of the process remains to be established. Upon the basis of our work, we will hazard an early hypothesis that the catalyst shape influences two important factors that contribute to etching direction in MaCE. First, because MaCE involves the

transfer of holes (h^+) from the metal to the silicon, the hole (h^+) rich regions will be those in intimate contact with the silicon, and as the silicon is etched away, the areas of the catalyst in contact with the silicon can vary with time but will be heavily dependent on catalyst shape. Thus, the shape of the dissolved silicon is dependent on the catalyst shape. Second, it has been proposed that electrophoresis resulting from electric field generated across the metal catalyst between the cathode and the anode is responsible for catalyst mobility.[26] As the shape of the catalyst changes, the electric field and the net force and moments due to that electric field will also change as different sections of the catalyst act as an anode or cathode. For example, the net force along the axis of the Ag nanorod is expected to be lower than that perpendicular to the axis due to the fact that anode and cathode run the entire length of the rod, providing a large force in the radial direction which can dominate any force from an electric field along the axis.

Overall, we have shown that MaCE is capable of fabricating, complex, controllable nano-, submicrometer, and micrometer sized features with resolutions on the order of tens of nanometers or less and with very smooth walls. MaCE offers a new method to fabricate nanostructures with distinct advantages as compared to existing technologies. AFM measurements of these structures showed aspect ratios that, while 50:1 aspect ratios have not yet been achieved, MaCE nanostructures are comparable with standard DRIE aspect ratios of ~10:1 but with distinct advantages. Foremost, in contrast to DRIE, the side walls of channels in MaCE are extremely smooth and primarily depend on the roughness of the catalyst particle with secondary dependence on etchant composition. As such, MaCE could have important applications for photonic devices and metamaterials, where roughness and other imperfections greatly reduce device efficiency. A second advantage to MaCE is the fact that the catalyst remains at the bottom of the hole and is available as a nucleation site for the growth of other materials using such processes as electroless deposition. Unlike standard evaporative methods to fill templates, *in situ* particle growth within the MaCE template will allow complex 3D shapes to be filled and multiple discrete layers of materials could be laid down without having to worry about constricting effects due to deposition on side walls. This will enable scientists to fabricate ever more complex nanostructures for both study and device application. The third and most obvious benefit of MaCE is that the catalyst moves as it etches, and therefore, unlike with other etching technologies, creating complex 3D shapes is possible and once the rules governing etching mechanics are determined, we expect to fabricate even more complex structures than the cycloids, sloping channels, and spiral structures reported in this study.

The final point that we would like to iterate is that this process is still in its infancy and a considerable amount of research on the fundamental properties that govern etching mechanics is necessary before MaCE will be ready for device fabrication. As such, one of the primary goals of this paper is to not only demonstrate the potential for MaCE as a new nanofabrication technology with novel capabilities but also encourage other scientists to also explore this process and help bring this technology to a reality.

EXPERIMENTAL SECTION

Silicon Wafer Preparation. All samples were prepared on 100 mm single side polished, p-type (1−100 Ω) single-crystal (100) silicon wafers. The wafers were cleaned at room temperature for 20 min using a piranha solution of 4:1 by volume of H_2SO_4 (95−98 wt %) and H_2O_2 (30 wt %). The Si pieces were then rinsed with distilled H_2O three times followed by a 3 min immersion in a dilute 1:100 HF (Alrich, 49 wt %) and rinsed three more times with distilled H_2O then dried with compressed air. For Ag nanorod samples, the silicon wafer was cleaved into ~1 × 6 cm^2 pieces prior to cleaning, while for EBL-patterned Au samples, the wafer was cleaned prior to patterning, patterned using the EBL, and then cleaved into ~1 × 1 cm^2 samples.

Ag Nanorod Synthesis. Ag nanorods were synthesized using a slightly modified ethylene glycol method described by Xia *et al.*[25] with $KAuCl_4$ used as the seed solution instead of $PtCl_2$. Twenty milliliters of ethylene glycol (BDA 99%) was heated to 160 °C in a 100 mL three-port round-bottom flask in a silicon bath with a 1 m water cooled condensation column attached to the center port. A 25.4 mm magnetic stir bar was used to stir the solution at 500 rpm. A 0.3 mM solution of $KAuCl_4$ (Aldrich 99.995%) made by dissolving 0.5 mg of $KAuCl_4$ in 2 mL of ethylene glycol and then added dropwise to the heated ethylene glycol. After ~4 min, a 20 mL, 0.59 M ethylene glycol solution of $AgNO_3$ (0.200 g, Aldrich, 99+%) and 10 mL of ethylene glycol solution of poly(vinyl pyrrolidone) (PVP, 0.550 g, Aldrich, $M_W \approx$ 29 000) was added dropwise to the ethylene glycol containing gold seeds.

This reaction was kept at temperatures between 160 and 165 °C for ~60 min. The solution was cooled to room temperature, diluted 2:1 with ethanol (VWR, denatured), and then centrifuged at 5000 rpm for 30 min to remove the ethylene glycol and excess PVP. The supernatant was removed using a plastic pipet, and the remaining Ag nanorod precipitate was diluted using ethanol and dispersed by sonication for 3 min. This process was repeated at least six times until the supernatant remained clear with centrifuge speeds ranging from 2000 to 5000 rpm. The synthesized and centrifuged Ag nanorods are then diluted with ethanol to form a light, slightly colored solution and dispersed onto a cleaved piece of cleaned silicon wafer using a 2 mL pipet with 1−2 drops of solution per cm^2 of Si such that the solution formed a thin film that did not break apart as the ethanol evaporated off the Si at room temperature. The Si piece was placed into a UV & Ozone Dry Stripper (Samco, model UV-1, 0.5 mL/min O_2) for 5 to 8 min. Depending on position in the UV−ozone stripper, time, and particle size, the PVP was completely or partially removed without damaging the Ag nanorods, not removed at all, or damaged the Ag nanorods. Ag nanorods with the PVP removed participated in MaCE.

Ag Nanodonut Synthesis. Ag nanodonuts were synthesized using the same solution based method as detailed in the Ag Nanorod Synthesis with a couple modifications. First, the reaction was conducted at 170 °C instead of 160 °C. Second, the solution was separated and cleaned *via* centrifugation using the same conditions and then stored as an ethanol solution for 1 month. The particles were then diluted using ethanol and dispersed onto a cleaned silicon wafer using a plastic pipet and then placed

into a UV & Ozone Dry Stripper (Samco, model UV-1, 0.5 mL/min O_2) for 5 to 7.5 min. Depending on position in the UV−ozone stripper, time, and particle size, a portion of the submicrometer Ag particles and Ag nanorods is distorted in the process to form Ag nanodonuts and nanoracetracks (roughly truncated circles). This process also removes any PVP capping agent and cleans the catalyst for MaCE.

PVP removal using UV−ozone was found to be dependent on position and time within the UV−ozone stripper. Below are graphs showing average Ag nanorod quality (arbitrary scale) and Ag nanorod etching quality *versus* radial distance from the center of the UV−ozone stripper along with representative SEM images from each section. SI-Figure 2 (Supporting Information) shows the Ag nanorod quality after UV−ozone before MaCE; positive values indicate good PVP removal, while negative values indicate Ag nanorod damage. SI-Figure 3 shows the etching quality after MaCE. Positive values indicate straight channels, while negative values indicate damaged nanorods, excess surface damage; 0 indicates no etching.

EBL-Patterned Catalysts. Four inch wafers were first cleaned using the same procedure as those used for Ag nanorod etching and then coated with a 180 nm positive electron resist of polymethyl methacrylate (PMMA). The pattern was exposed using a JEOL JBX-9300FS EBL system at 100 kV accelerating voltage and 50 pA current and cured. Ten nanometers of Ti and 50 nm of Au were deposited on the developed pattern using a CVC E-beam evaporator followed by a 30 min lift-off bath in 80 °C in *n*-methyl pyrrolidone to remove the unwanted metallization and PMMA, rinsed with acetone, and dried with N_2 gas. Internal tests showed that the Ti adhesion layer slows the etching rate so all EBL samples were etched for 40 min under $\rho = 90$ and 40 etchants. Au nanogrids were also etched with $\rho = 60$ to show 3D spiral etching.

Acknowledgment. We thank the National Science Foundation for their financial support (#0800849). We also thank Joel Pikarsky, Devin Brown, and Nicole Devlin of the Nanotechnology Research Center along with Yolande Berta and Todd Walters of the Center for Nanocharacterization at the Georgia Institute of Technology. Finally, we also thank Jack Moon, Rongwei Zhang, and Qizhen Liang.

Supporting Information Available: More detailed materials and methods section including silicon wafer cleaning, Ag nanorod and nanodonut synthesis, PVP removal using UV−ozone and thermal decomposition, position dependence of PVP removal using UV−ozone, EBL deposition, EBL patterns, rotating Au nanolines, and higher resolutions of all figures presented. This material is available free of charge *via* the Internet at http://pubs.acs.org.

REFERENCES AND NOTES

1. Ito, T.; Yamada, T.; Inao, Y.; Yamaguchi, T.; Mizutani, N. Fabrication of Half-Pitch 32 nm Resist Patterns Using Near-Field Lithography with a-Si Mask. *Appl. Phys. Lett.* **2006**, *90*, 1–3.
2. Koynov, S.; Brandt, M.; Stutzmann, M. Black Nonreflecting Silicon Surfaces for Solar Cells. *Appl. Phys. Lett.* **2006**, *88*, 203107-1–203107-3.
3. Weiss, S. M.; Haurylau, M.; Fauchet, P. Tunable Photonic Bandgap Structures for Optical Interconnects. *Opt. Mater.* **2005**, *27*, 740–744.
4. Ben, Y.; Gianchandani, Y.; Peterson, G.; Bergstrom, P.; Li, G.; Plummer, D.; Borboni, A.; Löfdahl, L.; Sobhan, C.; Muntz, E. *et al. Mems Applications*; Gad-el-Hak, M., Ed.; CRC: Boca Raton, FL, 2005; pp 1−568.
5. Yamada, K.; Fukuda, H.; Tsuchizawa, T. All-Optical Efficient Wavelength Conversion Using Silicon Photonic Wire Waveguide. *IEEE Photonics Technol. Lett.* **2006**, *18*, 1046–1048.
6. Boltasseva, A.; Shalaev, V. M. Fabrication of Optical Negative-Index Metamaterials: Recent Advances and Outlook. *Metamaterials* **2008**, *2*, 1–7.
7. Huczko, A. Template-Based Synthesis of Nanomaterials. *Appl. Phys. A* **2000**, *70*, 365–376.
8. Karniadakis, G.; Beşkök, A.; Rao Aluru, N. *Microflows and Nanoflows: Fundamentals and Simulation*; Springer: New York, 2005; pp 1−817.
9. Gupta, A.; Denton, J. P.; Mcnally, H.; Bashir, R. Novel Fabrication Method for Surface Micromachined Thin Single-Crystal Silicon Cantilever Beam. *Microelectromech. Syst.* **2003**, *12*, 185–192.
10. Kovacs, G. T. A.; Maluf, N. I.; Petersen, K. E. Bulk Micromachining of Silicon. Paper presented at the *Proceedings of the IEEE*; pp 1536−1551.
11. Cui, Z. *Nanofabrication: Principles, Capabilities and Limits*; Springer: New York, 2008; pp 52−54, 72.
12. Morton, K. J.; Nieberg, G.; Bai, S.; Chou, S. Y. Wafer-Scale Patterning of Sub-40 nm Diameter and High Aspect Ratio (>50:1) Silicon Pillar Arrays by Nanoimprint and Etching. *Nanotechnology* **2008**, *19*, 1–6.
13. Chattopadhyay, S.; Li, X.; Bohn, P. W. In-Plane Control of Morphology and Tunable Photoluminescence in Porous Silicon Produced By Metal-Assisted Electroless Chemical Etching. *J. Appl. Phys.* **2002**, *91*, 6134–6140.
14. Gorostiza, P.; Díaz, R.; Anbu Kulandainathan, M. Simultaneous Platinum Deposition and Formation of a Photoluminescent Porous Silicon Layer. *J. Electroanal. Chem.* **1999**, *469*, 48–52.
15. Huang, Z.; Zhang, X.; Reiche, M.; Liu, L.; Lee, W.; Shimizu, T.; Senz, S.; Goesele, U. Extended Arrays of Vertically Aligned Sub-10 nm Diameter [100] Si Nanowires By Metal-Assisted Chemical Etching. *Nano Lett.* **2008**, *8*, 3046–3051.
16. Xiu, Y.; Hess, D. W.; Wong, C. P.; Preparation of Multi-Functional Silicon Surface Structures for Solar Cell Applications. Paper presented at the *Electronic Components and Technology Conference*; pp 2117−2122.
17. Xiu, Y.; Zhang, S.; Yelundur, V.; Rohatgi, A.; Hess, D. W. Superhydrophobic and Low Light Reflectivity Silicon Surfaces Fabricated By Hierarchical Etching. *Langmuir* **2008**, *24*, 10421–10426.
18. Chartier, C.; Bastide, S.; Lévy-Clément, C. Metal-Assisted Chemical Etching of Silicon in HF-H_2O_2. *Electrochim. Acta* **2008**, *53*, 5509–5516.
19. Tsujino, K.; Matsumura, M. Morphology of Nanoholes Formed in Silicon By Wet Etching in Solutions Containing HF and H_2O_2 At Different Concentrations Using Silver Nanoparticle as Catalysts. *Electrochim. Acta* **2007**, *53*, 28–34.
20. Lee, C. L.; Tsujino, K.; Kanda, Y.; Ikeda, S.; Matsumura, M. Pore Formation in Silicon By Wet Etching Using Micrometre-Sized Metal Particles as Catalysts. *J. Mater. Chem.* **2008**, *18*, 1015–1020.
21. Tsujino, K.; Matsumura, M. Helical Nanoholes Bored in Silicon By Wet Chemical Etching Using Platinum Nanoparticles as Catalyst. *Electrochem. Solid-State Lett.* **2005**, *8*, C193–C195.
22. Tsujino, K.; Matsumura, M. Boring Deep Cylindrical Nanoholes in Silicon Using Silver Nanoparticles as a Catalyst. *Adv. Mater.* **2005**, *17*, 1045–1047.
23. Chun, I. S.; Chow, E. K.; Li, X. Nanoscale Three Dimensional Pattern Formation in Light Emitting Porous Silicon. *Appl. Phys. Lett.* **2008**, *92*, 191113.
24. Reimer, L. *Scanning Electron Microscopy: Physics of Image Formation and Microanalysis*; Hawkes, P., Ed.; Springer-Verlag: New York, 1998; pp 230−240.
25. Sun, Y.; Gates, B.; Mayers, B.; Xia, Y. Crystalline Silver Nanowires By Soft Solution Processing. *Nano Lett.* **2002**, *2*, 165–168.
26. Peng, K.; Lu, A.; Zhang, R.; Lee, S. Motility of Metal Nanoparticles in Silicon and Induced Anisotropic Silicon Etching. *Adv. Funct. Mater.* **2008**, *18*, 3026–3035.
27. Paxton, W. F.; Kistler, K. C.; Olmeda, C. C.; Sen, A.; St Angelo, S. K.; Cao, Y. Y.; Mallouk, T. E.; Lammert, P. E.; Crespi, V. H. Catalytic Nanomotors: Autonomous Movement of Striped Nanorods. *J. Am. Chem. Soc.* **2004**, *126*, 13424–13431.